Energy Storage Properties of Sr and Zr Doped Barium Titanate

Dissertation submitted to
Visvesvaraya National Institute of Technology, Nagpur
In partial fulfillment of the requirements for the award of
the degree

Master of Science
in
Physics

by

Tushar Belkhede (MS23PHY004)

under the guidance of

Dr. Oroosa Subohi

Department of Physics
Visvesvaraya National Institute of Technology
Nagpur 440010 (India)
May 2025

Energy Storage Properties of Sr and Zr Doped Barium Titanate

Dissertation submitted to
Visvesvaraya National Institute of Technology, Nagpur
In partial fulfillment of the requirements for the award of
the degree

Master of Science
in
Physics

by

Tushar Belkhede (MS23PHY004)

under the guidance of

Dr. Oroosa Subohi

Department of Physics
Visvesvaraya National Institute of Technology
Nagpur 440010 (India)

May 2025

© Visvesvaraya National Institute of Technology (VNIT) 2025

VISVESVARAYA NATIONAL INSTITUTE OF TECHNOLOGY, NAGPUR

DEPARTMENT OF PHYSICS

Dissertation approval sheet

Dissertation titled "**Energy Storage Properties of Sr and Zr Doped Barium Titanate**" by **Tushar Belkhede** is approved for the degree of Master of Science in Physics.

_____ (*Name*:) **Supervisor**	_____ (*Name*:) **External Examiner**

_____

(*Name*:)

Chairman

Visvesvaraya National Institute of Technology, Nagpur

Department of Physics

Declaration

I, Tushar Belkhede, hereby declare that this dissertation titled "**Energy Storage Properties of Sr and Zr Doped Barium Titanate**" is carried out by me in the Department of Physics of Visvesvaraya National Institute of Technology, Nagpur. The work is original and has not been submitted earlier whole or in part for the award of any degree/diploma at this or any other Institution / University.

Tushar Belkhede

Date:

Certificate

This to certify that the dissertation titled "**Energy Storage Properties of Sr and Zr Doped Barium Titanate**" is submitted by **Tushar Belkhede** in partial fulfillment of the requirements for the award of the degree of **Master of Science in Physics**, VNIT Nagpur. The work is comprehensive, complete and fit for final evaluation.

Dr. Oroosa Subohi
Assistant Professor
Department Of Physics
VNIT, Nagpur

Head, Department of Physics
VNIT, Nagpur
Date:

Visvesvaraya National Institute of Technology, Nagpur

Department of Physics

Non-Plagiarism Certificate

Certified that M.Sc. Dissertation titled "**Energy Storage Properties of Sr and Zr Doped Barium Titanate**" submitted by **Tushar Belkhede**, Enrollment No. **MS23PHY004**, ID No. **30093,** has been checked for plagiarism using TURNITIN software, and an overlap is found within prescribed limits (<30%). A summary of the report is given below:

Tushar Belkhede

(MS23PHY004)

ID No. 30093

Dr. Oroosa Subohi,

Assistant Professor

Department of Physics

VNIT, Nagpur

ACKNOWLEDGEMENTS

First and foremost, I express my deepest gratitude to the Almighty God for his continuous guidance, blessings, and grace throughout my life. Without his divine support, the successful completion of this project would not have been possible.

I would like to sincerely thank my project supervisor, ***Dr. Oroosa Subohi****, for accepting me as his M.Sc. project student and for his invaluable support, insightful guidance, and constant encouragement. His mentorship, patience during difficult phases, and generous support in terms of time, ideas, and resources played a pivotal role in the successful completion of this dissertation.*

My heartfelt thanks go to ***Mr. Amiya Ranjan Sahoo****, a member of my project progress committee, for her thoughtful suggestions, critical evaluations, and valuable feedback, which significantly enhanced the quality of my experimental work and research progress.*

I am also grateful to ***Professor Prem Lal Patel****, Director, VNIT, Nagpur, for providing the necessary research infrastructure, including laboratory, library, and characterization facilities, which were instrumental in the execution of my project.*

I extend my thanks to all the ***faculty members of the Department of Physics*** *for their constant support and willingness to help whenever approached during different stages of the project.*

On a personal note, I would like to express my immense love and gratitude to my father, Mr. Bhimrao Belkhede, whose unwavering belief in me, emotional strength, and endless sacrifices have been the backbone of my journey. He is truly my greatest inspiration. I am equally thankful to my mother, Mrs. Dwarka Belkhede, for her constant encouragement and moral support..

Thank you

Tushar Belkhede

ABSTRACT

The increasing demand for environmentally sustainable and high-performance dielectric materials has intensified research in lead-free ferroelectrics. This thesis focuses on the synthesis and characterization of strontium (Sr) and zirconium (Zr) co-doped barium titanate ($BaTiO_3$), forming the ceramic compound $Ba_{0.7}Sr_{0.3}Zr_xTi_{1-x}O_3$ (BSZT), as a promising alternative to traditional lead-based materials such as PZT. The primary objective of this work is to enhance the dielectric and energy storage properties of $BaTiO_3$ by substituting Sr at the A-site and Zr at the B-site of the perovskite structure, utilizing a conventional solid-state reaction method.

Three different compositions of $Ba_{0.7}Sr_{0.3}Zr_xTi_{1-x}O_3$ (BSZT) with varying Zr content (x = 0.04, 0.08, 0.12) were synthesized and subjected to structural, dielectric, and ferroelectric analysis. X-ray diffraction (XRD) confirmed the formation of a pure perovskite phase, and Rietveld refinement revealed an increase in lattice parameters with higher Zr doping, attributed to the larger ionic radius of Zr^{4+} compared to Ti^{4+}. Raman spectroscopy further validated the lattice distortion due to co-doping. Dielectric measurements demonstrated a high dielectric constant and low loss at low frequencies, while Zr doping enhanced frequency stability and reduced dielectric loss. Ferroelectric P-E loop analysis confirmed the ferroelectric nature of BSZT ceramics, with the composition x = 0.12 achieving the highest recoverable energy density (0.106 J/cm³) and efficiency (88%).

The results affirm that Sr and Zr co-doping significantly improves the energy storage performance and dielectric reliability of $BaTiO_3$ ceramics, making BSZT a strong candidate for applications in multilayer ceramic capacitors (MLCCs) and advanced energy storage systems. Future work may explore further compositional optimization, thin-film synthesis, and rare-earth doping to push the performance limits of BSZT-based materials.

LIST OF FIGURES

Figure No.	Figure title	Page no.
1.1	Ferroelectric material as a function of temperature	6
1.2	The Ideal Structure of ABO_3 Perovskite Compounds	7
1.3	Representation of the tetragonal tungsten bronze (TTB) structure	9
1.4	Structure of $A_2B_2O_7$ pyrochlore	10
1.5	Bismuth-based layered perovskite structures	11
1.6	Work plan	16
2.1	Mortar and pestle used for synthesis of BSZT ceramics	18
2.2	Solid state reaction synthesis route for preparing BSZT ceramics.	19
2.3	Schematic representation of interaction of X-rays with crystal planes	21
2.4	Illustration of various unit cells types with corresponding lattice parameters for perovskite structure	21
2.5	Energy transitions in Infrared absorption, Rayleigh, Stokes, and Anti-Stokes Raman scattering	23
2.6	P-E hysteresis loop showing the nonlinear relationship between polarization and electric field in ferroelectric materials.	26

2.7	High-resolution X-Ray diffractometer	28
2.8	Raman Spectrometer	28
2.9	P-E loop Set Up	29
3.1 a)	XRD pattern	31
3.1 (b-d)	Rietveld refinement of $Ba_{0.7}Sr_{0.3}Zr_xTi_{1-x}O_3$ ceramics with varying Zr as (x=0.00, 0.04, 0.08, 0.12)	31
3.2	Raman spectra for $Ba_{0.7}Sr_{0.3}Zr_xTi_{1-x}O_3$ (x=0.04, 0.08, 0.12) at room temperature.	33
3.3(a-b)	Variation of dielectric constant and dielectric loss with frequency respectively	33
3.4	PE hysteresis loop of prepared $Ba_{0.7}Sr_{0.3}Zr_xTi_{1-x}O_3$ samples with varying Zr as (x=0.04, 0.08, 0.12)	34
3.5 (a-c)	Energy storage density plot for prepared $Ba_{0.7}Sr_{0.3}Zr_xTi_{1-x}O_3$ ceramics (x=0.04, 0.08, 0.12)	35

LIST OF TABLES

Table No.	Table title	Page no.
1	Literature Survey On Energy Storage Properties Of Barium Titanate Based Ceramics	14
3.1	lattice parameters and volume of $Ba_{0.7}Sr_{0.3}Zr_xTi_{1-x}O_3$ (x=0.04, 0.08, 0.12)	32

INDEX

S.No.	Title	Page No.
	Abstract	i
	List of Figures	ii
	List of tables	iv
CHAPTER I		
INTRODUCTIONS, LITERATURE SURVEY AND OBJECTIVES		
1.1	General Introduction	1
1.2	Ferroelectric Materials	3
	1.2.1 Polarization	3
	1.2.2 Spontaneous Polarization	4
	1.2.3 Hysteresis Loop	4
1.3	Types of Ferroelectric Materials	6
	1.3.1 Perovskite-Type Ferroelectrics	7
	1.3.2 Tungsten Bronze-Type Ferroelectrics	8
	1.3.3 Pyrochlore Structured Ferroelectrics	9
	1.3.4 Bismuth Layer Structure Ferroelectrics	10
1.4	Literature Survey	11
	1.4.1 Introduction to Barium Strontium Zirconium Titanate (BSZT)	11
1.5	Objectives	15
1.6	Work Plan	16
CHAPTER II		
EXPERIMENTAL PROCEDURE AND PROPERTIES STUDIED		
2.1	Introduction	17
2.2	Synthesis route used	17

2.3 Characterization Techniques Used 20
2.3.1 X-ray Diffraction 20
2.3.2 Rietveld Refinement 22
2.3.3 Raman Spectroscopy 23
2.3.4 Dielectric characterization 24

2.4 Instrumentation 28
2.4.1 X-ray Diffraction 28
2.4.2 Raman Spectrometer 28
2.4.3 P-E Loop measurement 29

CHAPTER III

RESULTS AND DISCUSSION

3.1 Introduction 30
3.2 X-ray Diffraction Analysis 30
3.3 Raman Spectroscopy 32
3.4 Dielectric Properties 33
3.5 Ferroelectric properties 34

CHAPTER IV

CONCLUSION AND FUTURE SCOPE

4.1 Conclusions 36
4.2 Future Scope 36

CHAPTER 1

INTRODUCTION AND LITERATURE SURVEY

1.1 General Introduction

In recent years, there has been considerable interest in ferroelectric and piezoelectric materials, particularly barium-based ceramics, due to their unique dielectric, structural, and ferroelectric properties. These materials are of paramount importance in various electronic applications, such as sensors, actuators, and Ferroelectric RAM (FeRAM), owing to their ability to undergo reversible polarization under the influence of an applied electric field. Lead-based ceramics such as lead zirconium Titanate (PZT) is the most widely used ferroelectric material worldwide. It offers high dielectric constant, strong ferroelectric behaviour and can be altered easily for specific applications like sensors, transducers, etc. However, the major disadvantage of PZT is that it contains more than 60% of lead which contains hazards during processing and has harmful environmental effects during disposal. Lead accumulates in living tissues and damages the brain and nervous system. Due to the above mentions harmful side effects of the lead zirconium titanate, there was a need to find an environment friendly alternative with almost similar or better ferroelectric and piezoelectric properties. Therefore, barium titanate was taken into account.

Barium titanate ($BaTiO_3$) is widely recognized for its exceptional ferroelectric and dielectric characteristics, making it a critical material in these technologies. The dielectric properties of $BaTiO_3$ are particularly noteworthy, as the material exhibits a high dielectric constant, which facilitates efficient energy storage and the development of high-performance capacitors. These properties are intricately linked to the structural phase transitions that $BaTiO_3$ undergoes at various temperatures, influencing its ferroelectric behavior. At room temperature, $BaTiO_3$ adopts a tetragonal crystal structure, with the spontaneous polarization aligned along one of the crystal axes. Furthermore, the ferroelectric properties of $BaTiO_3$ make it an ideal candidate for energy harvesting and data storage devices due to its strong dipole moment, piezoelectricity, and pyroelectricity. These attributes are crucial for devices that require precise control and efficiency.

However, despite the well-established dielectric and ferroelectric properties of $BaTiO_3$, there is an increasing need to enhance its performance and address challenges related to its structural stability under varying operating conditions [1].

Dielectric materials, in general, are insulators that polarize when exposed to an electric field, resulting in a shift in charge distribution and a reduction of the effective electric field within the material. This characteristic is essential in energy storage devices, where dielectrics enhance energy storage capabilities and improve overall efficiency. By allowing more charge to accumulate at a given voltage, dielectric materials increase the capacity of these devices. Materials such as glass, ceramics, and certain polymers are commonly used as dielectrics due to their ability to withstand electric fields while maintaining their insulating properties. These materials are crucial in optimizing the performance of various energy storage systems. Dielectric materials can be broadly classified into piezoelectric, pyroelectric, and ferroelectric materials [2].

Piezoelectric materials generate an electric charge when subjected to mechanical stress, as their internal crystal structure becomes polarized. Mechanical deformation can be induced by applying an electric field. Some of the examples of piezoelectric materials are Rochelle salt, quartz, and lead zirconate titanate (PZT) [3].

Pyroelectric materials exhibit a change in polarization when subjected to heating and demonstrate spontaneous polarization in the absence of an external electric field. This phenomenon arises from the asymmetry in their crystal structure. Some of the examples of pyroelectric materials are lithium tantalate, tourmaline, and triglycine sulfate (TGS) [4].

Ferroelectric materials are those that can reverse their spontaneous electric polarization when an external electric field is applied. These materials are fundamental in various applications that require the control of electric polarization. Some of the examples of ferroelectric materials are PZT and barium titanate [5].

In conclusion, the advancements in barium-based ceramics, particularly $BaTiO_3$, have significant implications for the development of next-generation energy storage devices,

sensors, actuators, and data storage devices. Ongoing research in the enhancement of their properties through structural modifications, doping, and compositional engineering will continue to improve their performance and broaden their scope of application in various high-tech industries**.**

1.2 Ferroelectric Materials

These materials exhibit spontaneous electric polarization and when exposed to an external electric field, can reverse their polarization. When an electric field is applied on such material, it can reverse the displacement of ions in the crystal lattice, which causes the polarization. It is important to note that the history of the polarization change with respect to applied electric field determines the hysteresis behaviour of ferroelectric materials. PZT, lead titanate, and barium titanate are few of the examples. Some of the important applications of ferroelectric materials include piezoelectric sensors, capacitors, and memory devices (FeRAM) [6]. The curie temperature is critical temperature in ferroelectrics. It is the temperature above which ferroelectric material loses its polarization and becomes paraelectric material.

Ferroelectric materials consist of domains, which are regions containing dipoles aligned in the same direction. The dipole orientation differs depending on the domain. As the material moves from the paraelectric to the ferroelectric phase, the development of ferroelectric domains mainly reduces mechanical strain energy and electrostatic energy from the depolarizing field. The roughly equal distribution of positive and negative charges in all materials makes them electrically neutral, however the distribution of these charges is not always uniform or symmetrical. A material creates an electric dipole moment when the centers of gravity of its positive and negative charge distributions do not line up. [7]

1.2.1 Polarization

Polarization is defined as the dipole moment per unit volume. It measures how much electric dipole moment is present in a given volume of a material. The relation between dielectric displacement and polarization is

$$\boldsymbol{D} = \boldsymbol{P} + \varepsilon_0 \boldsymbol{E} \qquad (1)$$

where ε_0 is permittivity in free space.

D is also called as flux density or dielectric displacement, which is the charge per unit area that moves across a conductor layer in an electric field. Electric field causes bound charges in dielectric materials to separate, creating a local dielectric dipole moment. In ferroelectric materials, P and D are non-linear functions of the electric field and are additionally influenced by the material's previous history.

The four basic mechanisms of polarization are:

1. Electronic or Induced Polarization

2. Ionic polarization

3. Orientational Polarization

4. Interfacial or Space charge Polarization

1.2.2 Spontaneous Polarization

The magnitude of polarization inside a single ferroelectric domain without the presence of an external electric field is known as spontaneous polarization. It is an essential characteristic of ferroelectric materials. However, it can be reoriented and reversed in such materials. Temperature affects spontaneous polarization. Spontaneous polarization reduces as the temperature rises because the dipoles in the domain become more energetic and deformed. Hence, it decreases with increase in temperature and vanishes at a certain temperature which is known as Curie Temperature. [8]

1.2.3 Hysteresis Loop

The ferroelectric crystal contains large regions with homogeneous polarization which are known as domains. Each domain has particular direction of polarization and these domains are separated by a domain wall from each other. Domain switching is the reversal of the

domain's polarization caused by a strong electric field. The PE (polarization versus electric field) curve is non-linear for ferroelectric materials. When an electric field is applied to ferroelectric materials, the randomly oriented dipoles in different domains try to align in the direction of electric field. This increases the polarization in the material until it saturates and the material becomes a single domain. Further when the external field is reduced, the polarization decreases. But even if the applied field is zero, polarization does not become zero. There is some polarization in the materials even after applied field is made to zero, this is known as remnant polarization. To make this polarization back to zero, a reverse field should be applied. This field which is required to make polarization zero is known as coercive field. This behaviour of polarization versus electric field in ferroelectric material forms a loop which is known as hysteresis loop [9]

1.2.4 Curie Temperature and Phase Transition

Ferroelectric materials exhibit ferroelectric properties only when the temperature is below a certain temperature known as Curie temperature. The material acts as paraelectric above this temperature. The spontaneous polarization ceases at the Curie temperature. At the Curie point, ferroelectric material undergoes a phase shift. The distortion brought on by altered crystal structure of the material causes the dielectric, optical, and thermal constants to exhibit anomalous behaviour close to the Curie temperature or transition temperature.

Curie Weiss Law:

It gives relation between dielectric constant and the temperature above curie temperature ($T>T_c$) in the ferroelectric crystal and is given as,

$$\varepsilon_r = \varepsilon_0 + c/(T-T_c) \qquad (2)$$

where,

ε_r is the dielectric constant

ε_0 is the permittivity in free space

c is the curie constant

T_c is the curie temperature

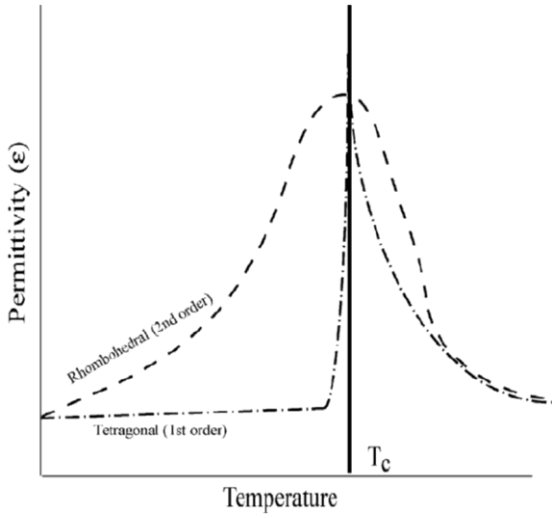

Fig. 1.1 Ferroelectric material as a function of temperature

1.3 Types of Ferroelectric Materials

Generally, ferroelectric materials are divided into four primary categories based on their unit cell structure. The arrangement of atoms within their unit cells and their crystallographic symmetry serves as the basis for these classifications. The four main types of ferroelectric materials are:

1. Perovskite-Type Ferroelectrics. e.g.: $BaTiO_3$, $PbTiO_3$

2. Tungsten Bronze-Type Ferroelectrics. e.g.: $Ba_5Nb_4O_{16}$, $Sr_5Nb_4O_{16}$

3. Hexagonal-Type Ferroelectrics e.g.: $LiNbO_3$, $LiTaO_3$

4. Bismuth Layer-Structured Ferroelectrics (BLSF). e.g.: $BiFeO_3$, $Bi_4Ti_3O_{12}$

1.3.1 Perovskite-Type Ferroelectrics

These are the ferroelectric materials which crystallizes in the perovskite structure, a particular kind of crystal lattice with the general formula ABO_3. Because of its exceptional qualities and extensive use in a wide range of electrical and optical applications, the perovskite structure is one of the most significant and thoroughly researched crystal structures in materials science.

The term "perovskite" refers to a specific mineral, while "perovskite structure" describes to material that has the same crystal structure as this mineral, typically represented by the general formula ABX_3. A and B are cations of different sizes in the general chemical formula ABX_3. The Vanderwaal's force and intermolecular contacts between ions in the crystal also play a role in the electric behaviour of this material, as does the size difference between these ions. These cations of varying sizes are joined by the anion X. The chemical formula for the perovskite structure of several oxides is ABO_3 [10]. An illustration of the perovskite structure is shown in the figure 1.2

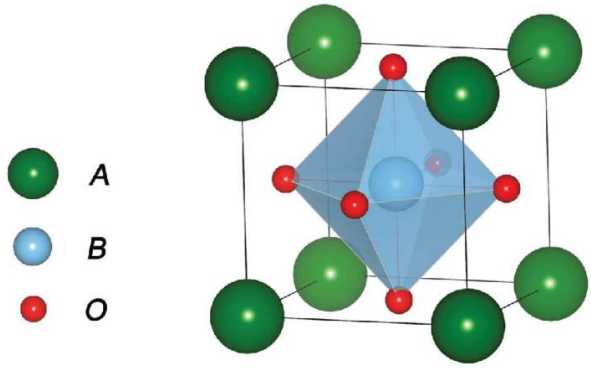

Fig 1.2 : The Ideal Structure of ABO_3 Perovskite Compounds

In most circumstances, the unit cell is slightly deformed due to constraints caused by the mixing of distinct ionic radii. Perovskite can have a wide range of intriguing properties, depending on which atoms or molecules are employed in the structure. Due to their crystal symmetry, perovskite-phase metal oxides have a variety of properties, including ferroelectric, dielectric, pyroelectric, and piezoelectric activity. Ferroelectric materials,

which are both pyroelectric and piezoelectric, are gaining a lot of attention due to the fact that applying an electric field can reorient their electric dipole. Above the material's curie temperature, these polar characteristics will also vanish, changing into a paraelectric phase, a nonpolar state.

The phase transition of perovskite phase minerals affects their physical characteristics. Controlling these characteristics is crucial to improving the quality of devices made from these materials because this phase transition is dependent on the chemical composition, the quantity of bulk and surface flaws, purity, sintering conditions, and grain size [11].

For example, **Barium Titanate** ($BaTiO_3$) exhibits perovskite structure which is the key material of our interest. it is discussed in brief in next sections.

1.3.2 Tungsten Bronze-Type Ferroelectrics

Compared to perovskites, tungsten bronze-type ferroelectrics are a class of ferroelectric materials with a more complex and flexible crystal structure. They are renowned for their potent ferroelectric, piezoelectric, and electro-optic qualities and are called after the mineral tungsten bronze (M_xWO_3). Bronze compounds such as lead meta niobate ($PbNb_2O_6$) and lead meta tantalate ($PbTa_2O_6$) are examples of such type of ferroelectric materials. At ambient temperature, the bronze form of these compounds has a meta stable structure. Since bronze typically is formed as solid solutions of at least two components, it appears that a certain amount of disorder can stabilize the structure [12]. Other compounds of relevance include $Ba_xSr_{1-x}Nb_2O_6$ and $Ba_2NaNb_5O_{15}$ in addition to $PbNb_2O_6$ and $PbTa_2O_6$.

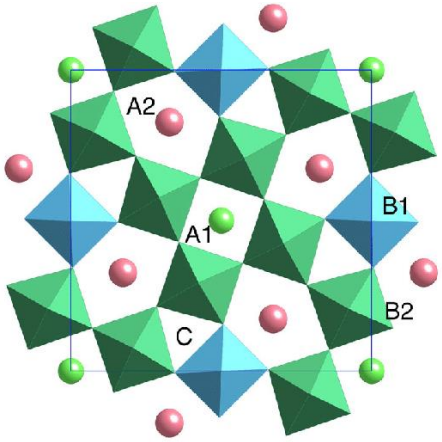

Fig1.3 Representation of the tetragonal tungsten bronze (TTB) structure [12]

The typical chemical formula is $(A_1)_2(A_2)_4(C)_4(B_1)_2(B_2)_8O_{30}$ in which A1, A2, and C are 12-, 15-, 9- fold coordinated interstitial sites in the crystal structure surrounded by oxygen anions. The 82 oxygen octahedra has a greater shape distortion than the B1 and B2 sites, which are both 6-fold coordinated interstitial sites inside oxygen octahedra. Actually, there are five distinct oxygen sites, which can be identified by the quantity and type of cations present. There are currently over a hundred ferroelectric materials that are members of the tungsten bronze family.

1.3.3 Pyrochlore Structured Ferroelectrics

Materials with the stoichiometric formula $A_2B_2O_7$ exhibit the pyrochlore structure. A trivalent "A" cation and a tetravalent "B" cation combine to generate pyrochlores, while they can also form in the $A^{2+}{}_2\ B^{5+}{}_2O_7$ stoichiometry. Pyrochlore compounds offer a wide range of properties due to their wide composition, and they have been utilized or are being proposed as materials for use in a variety of applications, including solid electrolytes [13]. Ferroelectric materials with a pseudo-pyrochlore structure, such $Ce_2Ti_2O_7$, $Sr_2Nb_2O_7$, $La_2Ti_2O_7$ (LTO), and $Nd_2Ti_2O_7$ (NTO), have a low dielectric constant, a high coercive field, and good thermal stability.

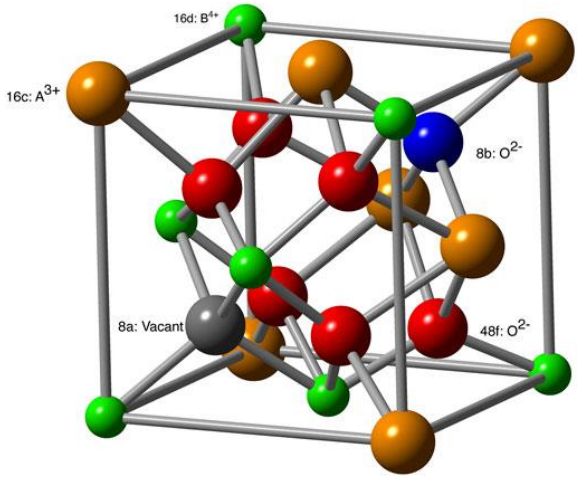

Fig 1.4 Structure of $A_2B_2O_7$ pyrochlore. Different crystallographic positions are labelled. For anion sublattice these are also indicated by different colours: 48*f* (red), 8*a* (grey, vacant site in stoichiometric pyrochlore) and 8*b* (blue)

1.3.4 Bismuth Layer Structure Ferroelectrics

Bismuth layer-structured ferroelectrics (BLSFs) are a class of materials distinguished by their unique layered perovskite-like structure, in which perovskite units alternate with bismuth oxide $(Bi_2O_2)^{2+}$ layers along the crystallographic *c*-axis. The general formula for these materials is $(Bi_2O_2)^{2+}(A_{n-1}B_nO_{3n+1})^{2-}$, where *A* and *B* represent metal cations such as strontium (Sr), calcium (Ca), barium (Ba), or titanium (Ti).

The layered structure of BLSFs provides excellent thermal and chemical stability, making them particularly well-suited for high-temperature applications. Ferroelectricity in these materials arises from the off-centering of *B*-site cations and distortion of the BO_6 octahedra, leading to spontaneous polarization. This polarization can be reversed by the application of an external electric field. The ferroelectric characteristics of materials such as $SrBi_2Ta_2O_9$ (SBT) and $Bi_4Ti_3O_{12}$ (BIT) have been thoroughly investigated among BLSFs [14].

These substances are perfect candidates for non-volatile ferroelectric random-access memory (FeRAM) systems because of their high Curie temperatures and

exceptional fatigue resistance. Furthermore, their directional dependency in dielectric and piezoelectric properties—which can be adjusted for particular applications—is a result of their anisotropic crystal structure. The goal of ongoing research is to improve the ferroelectric performance, stability, and compatibility of BLSFs with contemporary microelectronic production procedures by altering their composition and structure.

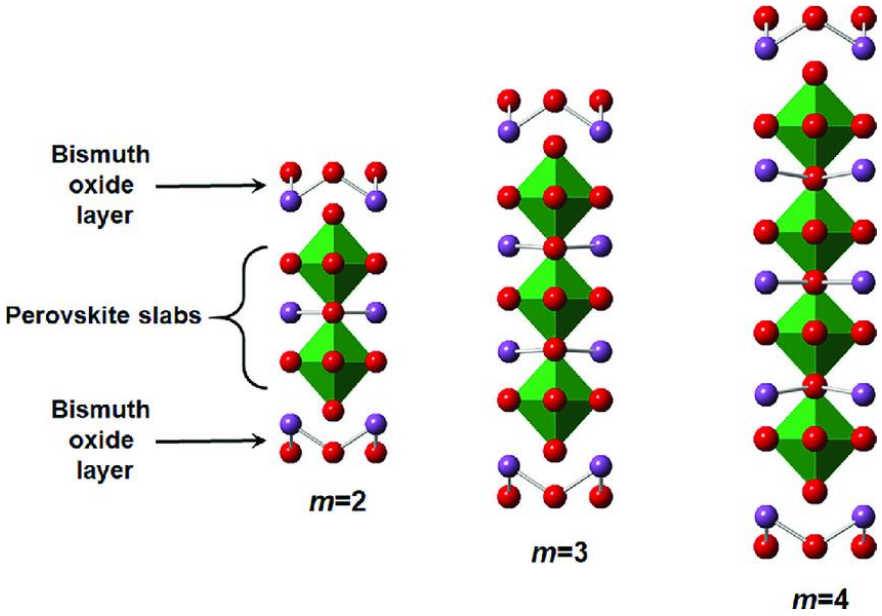

Fig. 1.5 Bismuth-based layered perovskite structures

1.4 Literature Survey

1.4.1 Introduction To Barium Strontinium Zirconium Titanate (BSZT)

Barium strontium zirconium titanate (BSZT) ceramics are a class of lead-free perovskite minerals known for their excellent dielectric and ferroelectric properties. $(Ba_{1-x}Sr_x)(Ti_{1-y}Zr_y)O_3$ is the usual representation of BSZT, where Sr and Zr are partial dopants for Ba and Ti, respectively. These dopings have a major impact on the electrical and structural characteristics of the material. Therefore BSZT is a viable option for high-performance dielectric materials, particularly in energy storage applications.

In this report, strontium is doped in place of barium in barium titanate ceramics because the ionic radius of strontium (Sr^{2+}) is lower than that of barium (Ba^{2+}). Sr lowers the tetragonality of the crystal structure and causes lattice distortion when it is substituted into the A-site of the perovskite lattice. This improves the material's dielectric stability and temperature dependability by causing the Curie temperature (T_c) to move nearer to room temperature.

However, zirconium is doped in place of titanium in barium titanate ceramics because zirconium (Zr^{4+}) ions are larger than titanium (Ti^{4+}) ions. When Zr is substituted into the B-site, the long range ferroelectric ordering is suppressed and the relaxor behaviour is improved. This results into better breakdown strength across a broad temperature range and increased energy storage density. When Sr and Zr dopings are combined, the result is a customized BSZT composition that strikes a balance between ferroelectricity, dielectric strength, and energy storage capacity. These changes make BSZT perfect for uses such as embedded capacitors, energy storage devices, and multilayer ceramic capacitors (MLCCs) by lowering dielectric loss and increasing recoverable energy density [15],[16]

$BaTiO_3$ (Barium Titanate)

$BaTiO_3$ exhibits a high dielectric constant (1200–1500) and low dissipation factor (<0.02), with energy density ranging from ~0.3–1.5 J/cm³ and a moderate maximum polarization of ~25 μC/cm². It is widely synthesized via solid-state or sol-gel routes, making it a classical and extensively studied ferroelectric material.

$Pb(Zr,Ti)O_3$ (PZT)

PZT is a versatile ferroelectric with a dielectric constant of 1000–1500 and dissipation factor between 0.01–0.03. It offers energy densities around 1–2 J/cm³ and high polarization (~30–40 μC/cm²). Synthesized through solid-state, sol-gel, or CVD methods, PZT remains a cornerstone in piezoelectric and actuator applications.

$BiFeO_3$ (BFO)

$BiFeO_3$ shows a relatively low dielectric constant (50–100) and a variable dissipation factor (0.01–0.05). Despite a lower energy density (~0.1–0.3 J/cm³), it boasts very high polarization values (60–100 μC/cm²). It is typically synthesized using sol-gel or hydrothermal techniques and is known for its multiferroic behavior.

HfO_2-based (doped)

Doped HfO_2-based materials exhibit low dielectric constants (20–30) and very low dielectric loss (~0.01), but can achieve impressive energy densities (~2–3 J/cm³) with polarization values of ~10–30 μC/cm². These are commonly synthesized via advanced methods like ALD and sputtering, making them ideal for miniaturized electronics.

$K_{0.5}Na_{0.5}NbO_3$ (KNN)

KNN materials offer a wide dielectric range (200–600), low dissipation factor (~0.02), and energy density around 1 J/cm³. Polarization values fall between ~25–35 μC/cm². These materials are typically prepared via solid-state or sol-gel methods and are considered promising lead-free alternatives for piezoelectric applications.

$SrBi_2Ta_2O_9$ (SBT)

SBT possesses a dielectric constant of 200–300 and low dielectric loss (~0.01–0.05), with energy densities between ~0.1–0.5 J/cm³ and polarization of ~15–25 μC/cm². Prepared by MOCVD or sol-gel techniques, SBT is valued for its fatigue-resistant ferroelectric properties in non-volatile memory applications.

$Pb(Mg_{1/3}Nb_{2/3})O_3$–$PbTiO_3$

This composite ferroelectric material combines $Pb(Mg_{1/3}Nb_{2/3})O_3$ (PMN) with $PbTiO_3$, yielding a moderate dielectric constant (200–400) and very low dissipation factor (<0.03). It offers a relatively high energy density (~5.0 J/cm³) and polarization (~30–35 μC/cm²), making it suitable for energy storage and actuator applications. The material is typically synthesized via chemical solution deposition (CSD) using spin-coating techniques, which support thin-film fabrication for miniaturized devices.

$BaZr_{0.4}Ti_{0.6}O_3$

This Zr-doped barium titanate variant exhibits a dielectric constant of around 300, low dielectric loss (~0.02), and a significantly high energy density (~8 J/cm³) with a polarization of ~40 μC/cm². The Zr substitution enhances relaxor-like behavior and breakdown strength. $BaZr_{0.4}Ti_{0.6}O_3$ is often prepared using pulsed laser deposition (PLD), enabling precise thin-film growth for advanced microelectronic and capacitor applications.

$(Na_{0.5}Bi_{0.5})_{1-x}Sr_xTiO_3$

This solid solution system offers a dielectric constant of ~500, a moderate dissipation factor (~0.03), high energy density (~9 J/cm³), and strong polarization (~45 μC/cm²). The presence of Sr modifies the perovskite lattice and improves dielectric stability. It is synthesized via solid-state or sol-gel methods, making it a promising lead-free ferroelectric material for energy storage and actuator technologies.

$Na_{0.5}Bi_{0.5}TiO_3$

$Na_{0.5}Bi_{0.5}TiO_3$ (NBT) is a well-known lead-free ferroelectric with a high dielectric constant (~1000), relatively higher dielectric loss (~0.04), and modest energy density (~1.2 J/cm³). It exhibits decent polarization (~38 μC/cm²) and is synthesized via the solid-state reaction method. NBT is often used in piezoelectric sensors and actuators due to its stable ferroelectric properties and environmental compatibility.

Table 1 : Literature Survey On Energy Storage Properties Of Barium Titanate Based Ceramics

Ferroelectric Material	Dielectric Constant (ε_r)	Dissipation Factor (Tan δ)	Energy Density (J/cm^3)	Maximum Polarization ($\mu C/cm^2$)	Synthesis Method	Reference
$BaTiO_3$ (Barium Titanate)	1200–1500	< 0.02	~0.3–1.5	~25	Solid-state, Sol-gel	[17]
$Pb(Zr,Ti)O_3$ (PZT)	1000–1500	~0.01–0.03	~1–2	~30–40	Solid-state, Sol-gel, CVD	[18]
$BiFeO_3$	50–100	~0.01–0.05	~0.1–0.3	~60–100	Sol-gel, Hydrothermal	[19]
HfO_2-based (doped)	20–30	< 0.01	~2–3	~10–30	ALD, Sputtering	[20]
$K_{0.5}Na_{0.5}NbO_3$ (KNN)	200–600	< 0.02	~1	~25–35	Solid-state, Sol-gel	[21]
$SrBi_2Ta_2O_9$ (SBT)	200–300	~0.01–0.02	~0.1–0.5	~15–25	MOCVD, Sol-gel	[22]
$Pb(Mg_{1/3}Nb_{2/3})O_3–PbTiO_3$	200–400	< 0.03	~ 5.0	~ 30–35	CSD + spin-coat	[23]
$BaZr_{0.4}Ti_{0.6}O_3$	~ 300	~ 0.02	~ 8	~ 40	Pulsed-laser deposition	[24]

$(Na_{0.5}Bi_{0.5})_{1-x}Sr_xTiO_3$	~ 500	~ 0.03	~ 9	~ 45	Solid-state sol-gel	[25]
$Na_{0.5}Bi_{0.5}TiO_3$	~ 1 000	~ 0.04	~ 1.2	~ 38	Solid-state	[26]

1.5 Objectives

The main objectives of this thesis report are listed below:

1) To synthesize Sr and Zr co-doped Barium Titanate (BSZT) ceramics using the solid-state route.

2) To study the effect of Sr and Zr doping on the structural, dielectric, and energy storage properties.

3) To optimize doping levels for enhanced recoverable energy density and dielectric constant

This study will help in developing efficient dielectric materials for advanced capacitor and energy storage applications.

1.6 Work plan

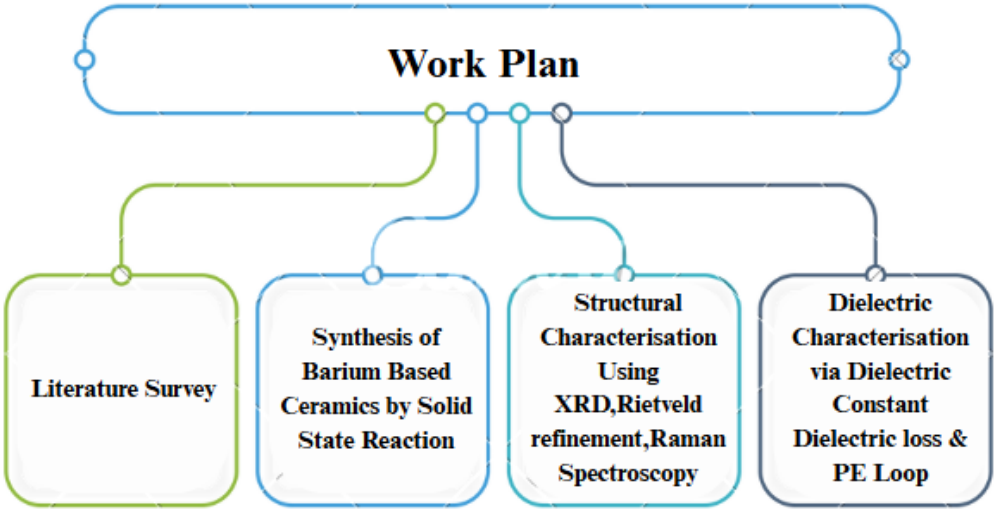
Work Plan
Literature Survey
Synthesis of Barium Based Ceramics by Solid State Reaction
Structural Characterisation Using XRD,Rietveld refinement,Raman Spectroscopy
Dielectric Characterisation via Dielectric Constant Dielectric loss & PE Loop

Fig 1.6 Work Plan

CHAPTER 2

EXPERIMENTAL PROCEDURE AND PROPERTIES STUDIED

2.1 Introduction

In this chapter, the explanation for synthesis route used (Solid State Reaction method) is given for the synthesis of barium strontium zirconium titanate ceramics. Also, the details of various characterization techniques that were studied for given sample are explained in brief such as XRD, Raman spectroscopy, dielectric characterisation, PE loop study, etc

Barium strontium zirconium titanate ceramics (BSZT) of different compositions of Zr were prepared for their structural and dielectric study. BSZT has a general formula $Ba_{0.7}Sr_{0.}3Zr_xTi_{(1-x)}O_3$. Three samples were prepared by varying Zr composition are given as

1) $Ba_{0.7}Sr_{0.3}Zr_{0.04}Ti_{0.96}O_3$

2) $Ba_{0.7}Sr_{0.3}Zr_{0.08}Ti_{0.92}O_3$

3) $Ba_{0.7}Sr_{0.3}Zr_{0.12}Ti_{0.88}O_3$

2.2 Synthesis route

In this work, the Sr and Zr doped Barium titanate powders were synthesized by using Solid State Reaction method.

A common and extensively used approach for the synthesis of a wide variety of inorganic materials, especially ceramics, is the solid-state reaction method, sometimes referred to as the ceramic method. Solid precursor powders, usually oxides, carbonates, or other inorganic compounds, are mixed in exact stoichiometric ratios using this technique. The desired phase is then formed by promoting interdiffusion and a chemical reaction between the constituents through high-temperature calcination of the mixture. Because of its ease

of use, affordability, and appropriateness for large-scale production, the solid-state reaction approach is preferred. It is still a fundamental synthesis method in solid-state chemistry and materials research, despite its drawbacks like longer reaction durations and the requirement for frequent grinding and fire to guarantee phase purity and homogeneity. [27]

Fig 2.1 Mortar and pestle used for synthesis of BSZT ceramics

The solid-state reaction method is used to create the BSZT ceramics. When it comes to synthesis, the solid-state reaction method is one of the most used and traditional methods. The solid-state reaction method's simplicity, affordability, and appropriateness for large-scale production are its main advantages. This process creates the required crystalline phase by combining and calcining the precursor powders at high temperatures. With the right processing parameter optimization, it provides strong control over phase purity and homogeneity, although typically requiring higher processing temperatures. Because it guarantees strong chemical compatibility between the constituent elements and permits exact stoichiometric control, the approach is especially advantageous for the synthesis of complicated oxide ceramics such as BSZT. Additionally, by improving the diffusion between the reactants, mechanical mixing and repeated calcination stages aid in the creation of a homogeneous microstructure and better densification in the final sintered ceramic.

Three samples of BSZT are made by solid state reaction method depending on the doping concentration of Zirconium. Barium carbonate, Strontium carbonate, Zirconium dioxide, and Titanium oxide were used as precursors for the synthesis of BSZT ceramics.

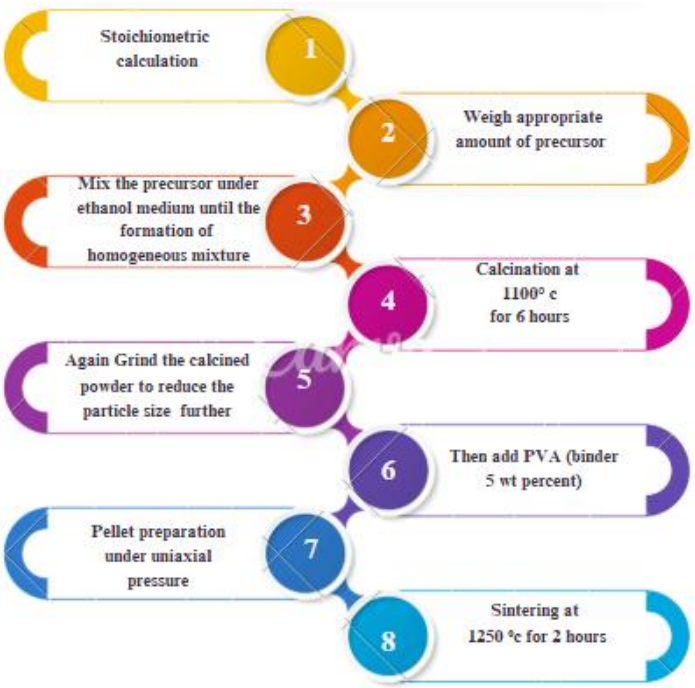
Stoichiometric calculation
1
2
Weigh appropriate amount of precursor
Mix the precursor under ethanol medium until the formation of homogeneous mixture
3
4
Calcination at 1100° c for 6 hours
Again Grind the calcined powder to reduce the particle size further
5
6
Then add PVA (binder 5 wt percent)
Pellet preparation under uniaxial pressure
7
8
Sintering at 1250 °c for 2 hours

Fig 2.2 Solid state reaction synthesis route for preparing BSZT ceramics.

At first the stoichiometric calculations were done for getting the exact amount of precursors for the required concentrations of dopant. These precursors were then weighed appropriately using 'scale-tec analytical weighing balance' as per the stoichiometric calculations. They were then mixed under ethanol medium and grinded for 7-8 discontinuous hours until the formation of homogeneous mixture. This mixture was then calcined at 1100°C for 6 hours to remove the volatile impurities, to initiate and drive solid state reaction and to achieve desired phase transition. The powder was again grinded to reduce its size further. Then PVA (binder) was added onto it which adheres the reactants

to each other and improve overall reaction efficiency. This powder was the pressed into pallets of 10mm diameter and 2mm thickness under 100 kg/cm^2 pressure using hydraulic pressure to improve the surface area for reaction and to improve homogeneity of the mixture. The pallets were sintered at 1250°C for 2 hours to densify the pallets, promoting atomic diffusion and reducing porosity. The final sintered sample were then sent for characterisation studies.

2.3 Characterization techniques used

2.3.1 X-Ray Diffraction

X-ray Diffraction (XRD) is a widely used, efficient technique for identifying the various phases present in crystalline materials. Beyond phase identification, it provides valuable information about the crystal structure, preferred orientation, average crystallite size, internal strain, degree of crystallinity, and potential defects within the material. The technique operates by directing X-rays at a sample and analyzing the way these rays are scattered at specific angles. The resulting diffraction pattern contains characteristic peaks, which arise due to constructive interference of X-rays reflected from parallel atomic planes in the crystal. This phenomenon is explained by **Bragg's Law**, represented by the equation:

$$\mathbf{n\lambda = 2d \sin\theta} \qquad \textbf{(}3\textbf{)}$$

where:

n is the order of diffraction,

λ is the wavelength of the X-rays,

d is the interplanar spacing (distance between atomic layers), and

θ is the angle of incidence.

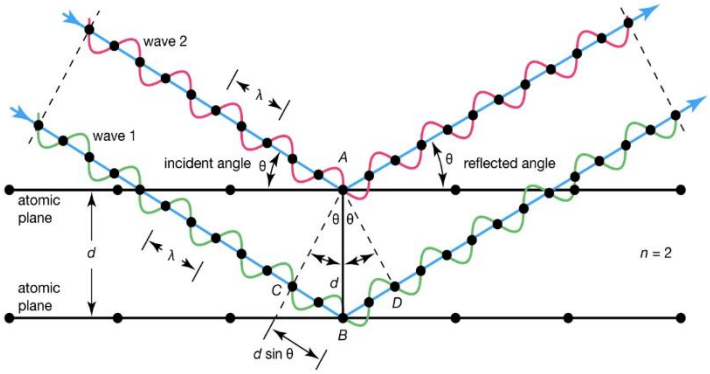

Fig 2.3 Schematic representation of interaction of X-rays with crystal planes

For diffraction to occur, the interatomic spacing must be on the order of the X-ray wavelength. By measuring and analyzing the positions and intensities of these peaks, one can determine the crystal structure, phase composition, and other important physical characteristics of the material [28].

X-ray diffraction patterns can be effectively used to monitor chemical reactions, as they are closely linked to the crystal symmetry and structural properties of a material, including phase purity and symmetry transitions. When the crystal structure changes during a reaction, it often leads to a change in symmetry, which is reflected in the XRD pattern.

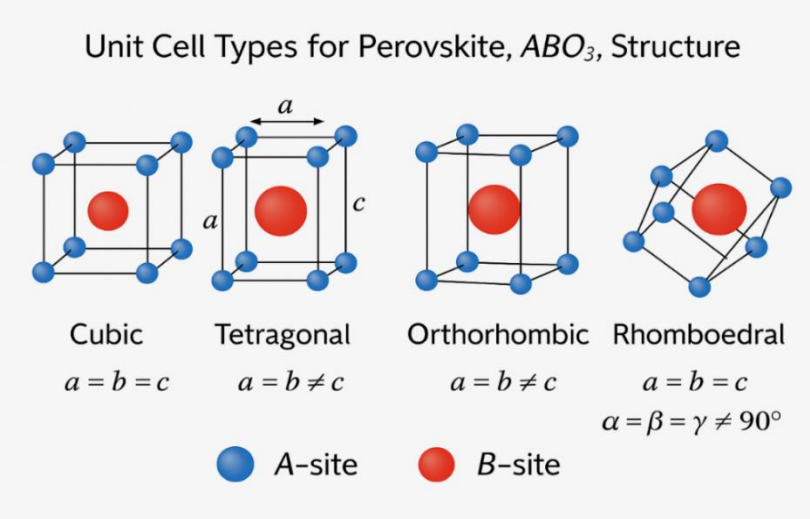

Fig 2.4 Illustration of various unit cells types with corresponding lattice parameters for perovskite structure

Such structural transitions alter the **d-spacings** between atomic planes, resulting in observable changes such as the **splitting** or **merging** of diffraction peaks, as illustrated in fig 2.4.

2.3.2 Rietveld refinement

A sophisticated technique for obtaining exact structural information from X-ray or neutron powder diffraction data is Rietveld refinement. By fine-tuning a structural model until the computed pattern closely resembles the observed one, this method fits the complete diffraction pattern rather than examining individual peaks.

Materials having overlapping peaks, intricate crystal structures, or numerous phases benefit greatly from this technique. The refining process entails changing variables like:

- Lattice constants,
- locations of atoms,
- vibrations caused by heat,
- effects produced by instruments, and
- microstructural elements such as crystallite size or strain.

Least-squares minimization is used to fit the data, minimizing the discrepancy between the calculated and observed intensities. Indicators like χ^2 (chi-squared), R_{wp} and R_p are used to gauge the fit's quality.

A successful refinement keeps the residual (difference) curve close to zero while the computed curve closely resembles the observed data.

High-quality diffraction data and a solid initial model are essential for Rietveld refining success. Rietveld refinement is essential for describing crystalline materials since it helps identify specific characteristics like atomic arrangements, site occupancies, and phase fractions in addition to phase identity [29].

2.3.3 Raman spectroscopy

Based on the inelastic scattering of monochromatic light, usually from a laser source, when it interacts with molecular vibrations or crystal lattice phonons, Raman spectroscopy is a powerful analytical technique that provides insights into the vibrational, rotational, and other low-frequency modes in a material. Unlike Rayleigh scattering, where the scattered light has the same energy as the incident light, Raman scattering involves a slight energy shift that gives each substance a molecular "fingerprint" that is specific to that substance. This technique is highly sensitive to chemical bonding, crystal symmetry, and molecular structure, making it ideal for: Identifying chemical compounds, studying crystallinity and phase transitions, probing defects and disorder in solids, and characterizing nanomaterials and thin films. The various vibrational modes are represented by the peaks that make up the Raman spectrum. The types of bonds, molecular symmetry, and stress or strain in solid materials are all revealed by these peaks.

Raman spectroscopy is non-destructive in nature and ability to be used in situ or via transparent containers are some of its main advantages. Raman spectroscopy is frequently used in solid-state materials research to examine temperature-dependent behaviors, phase purity, phonon confinement, and interactions between molecules or ions in a lattice [30]

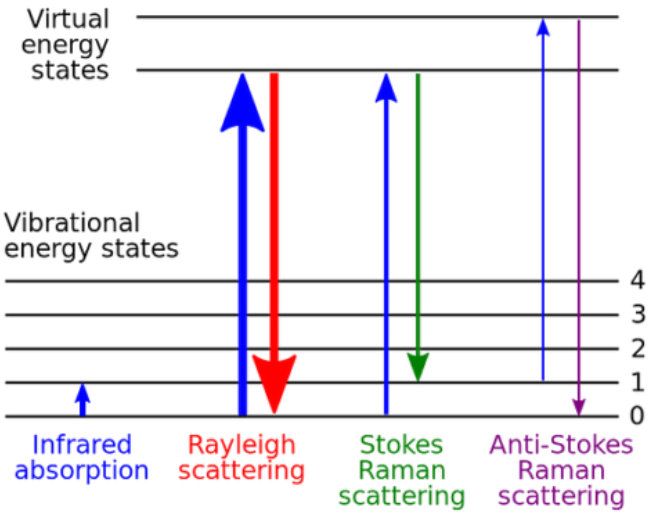

Fig 2.5 Energy transitions in Infrared absorption, Rayleigh, Stokes, and Anti-Stokes Raman scattering.

2.3.4 Dielectric characterization

Dielectric constant

The **dielectric constant**, also known as **relative permittivity (ε_r)**, describes a material's ability to store electrical energy and is a fundamental property of dielectric materials. It is defined as the ratio of the charge stored on electrodes separated by a dielectric material at a given voltage to the charge stored on identical electrodes separated by a vacuum.

Mathematically, it is expressed as:

$$\varepsilon_r = 1 + P / (\varepsilon_0 E) \quad (4)$$

Here, the dielectric constant ε_r is related to the **polarization (P)**—the induced dipole moment per unit volume—under an applied electric field **E**, and ε_0 is the permittivity of free space.

For an **alternating electric field**, the dielectric constant becomes complex and is written as:

$$\varepsilon_r = \varepsilon' - i\varepsilon'' \quad (5)$$

Where:

- ε' (real part) corresponds to the component in phase with the applied electric field and represents energy storage.

- ε'' (imaginary part) is 90 degrees out of phase and represents energy loss, typically due to dielectric absorption or resistive leakage.

The **dielectric constant varies with temperature**, and significant changes in permittivity can occur. As temperature increases, ε_r increases until reaching the **Curie temperature**, after which it drops sharply due to the loss of ferroelectric behavior.

Additionally, **frequency** affects permittivity. When a material is in a static electric field, it exhibits **static permittivity**. As the frequency of the applied voltage increases, the relative permittivity $\boldsymbol{\varepsilon_r}$ generally decreases [31].

Dielectric Loss (tan δ)

In dielectric materials, along with the **charging current**, there is also a **loss current** due to the long-range movement (migration) of charges. While the charging current ideally leads the applied voltage by **90 degrees (π/2 radians)**, real materials experience a phase lag because of energy dissipation.

When an **alternating (AC) electric field** is applied to a dielectric, two components of current arise:

- The **charging (or displacement) current**, which is associated with energy storage.
- The **loss current**, which flows through a resistive path and represents **energy dissipation**.

In practice, the **total current** leads the voltage by an angle slightly less than 90°, that is, **(90° – δ)**. The angle **δ** is known as the **loss angle** and reflects how much the dielectric deviates from ideal behavior [32].

The **dielectric loss** quantifies the **energy dissipated as heat** in the material and can arise from various physical processes such as:

- Electrical conduction,
- Dielectric relaxation,
- Dielectric resonance,
- Nonlinear loss mechanisms.

It is expressed as:

$$\boldsymbol{\tan\delta = \varepsilon''/\varepsilon'} \qquad (6)$$

Where:

- **ε′** is the real part of the dielectric constant (energy stored)
- **ε″** is the imaginary part (energy lost)

The **reciprocal** of the loss tangent is called the **quality factor (Q)**, which indicates how well the material stores energy relative to how much it loses [33] :

$$\mathbf{Q = 1/\tan\delta} \qquad (7)$$

P-E Hysteresis Loop in Ferroelectric Materials

P-E loop (Polarization vs. Electric Field loop) represents how the polarization of a material responds to an applied electric field at a given frequency. This loop is particularly important for **ferroelectric materials**, which exhibit **reversible spontaneous polarization**—meaning their polarization can be switched by applying an electric field in the opposite direction.

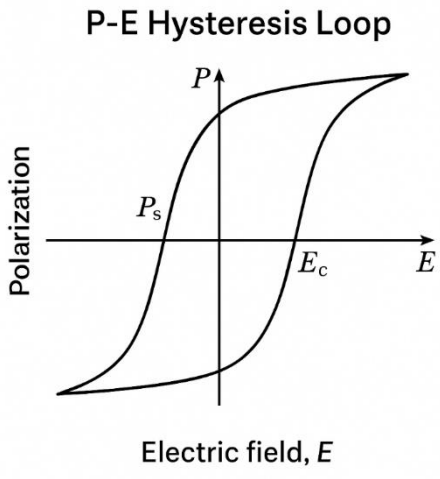

Fig 2.6 P-E hysteresis loop showing the nonlinear relationship between polarization and electric field in ferroelectric materials.

The relationship between polarization (**P**) and the electric field (**E**) is **non-linear**, and this behavior is captured by the **hysteresis curve** or **hysteresis loop**. This loop illustrates how

a ferroelectric material becomes polarized in one direction and then reverses polarization when the direction of the electric field is reversed.

Ferroelectric hysteresis has gained a lot of attention in recent years due to its application in **non-volatile memory devices**, especially using ferroelectric thin films.

When an electric field is applied, the polarization initially increases **linearly**, then **non-linearly** as the internal domains within the material begin to align with the field direction. Once most domains are aligned, the polarization reaches a **saturation point**, beyond which it cannot increase further despite increasing the field.[34]

As the field is gradually reduced to zero, the polarization also decreases. However, it doesn't return to zero. By extrapolating the linear part of the curve back to the polarization axis, we get the **spontaneous polarization (P_s)**. Even when the field is removed, some residual polarization, known as **remnant polarization (P_r)**, remains. This is usually less than P_s because some domains revert back due to internal strain or instability.

To reduce the net polarization to zero, a reverse electric field must be applied. The magnitude of this field is called the **coercive field (E_o)**. The coercive field is influenced by factors like **temperature** and the **frequency** of the applied field.

The **area enclosed by the P-E loop** represents the **energy lost as heat** during each cycle. This energy corresponds to what's required to reorient the domains back to their original state. An **ideal hysteresis loop** is symmetric, meaning the **positive and negative values** of coercive field and remnant polarization are equal [35]. However, in practice, the shape and features of the loop can be affected by multiple factors such as:

- Sample thickness
- Charge defects
- Mechanical stress
- Processing conditions
- Thermal treatment

2.4 Instrumentation

2.4.1 X-Ray Diffraction

The XRD patterns are obtained from a high-resolution X-Ray diffractometer (HRXRD, D8-Advance, Bruker, Germany) with Cu Kα radiation (λ =0.15406 nm)**.** The HRXRD system equipped with θ-θ gonio meter, copper X-ray source, Gobel mirror, double crystal monochromator and Lynxeye 1-D fast detector.

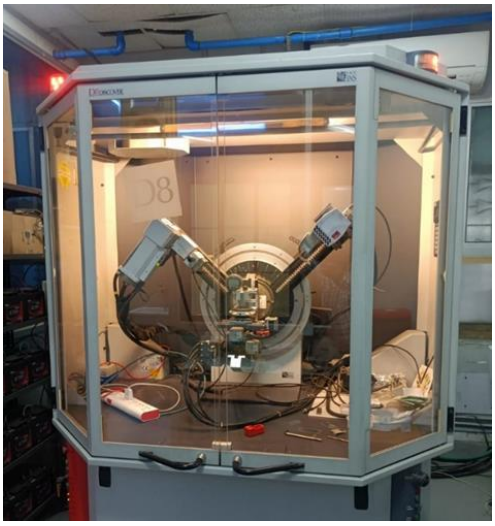

Fig. 2.7 High-resolution X-Ray diffractometer

2.4.2 Raman Spectrometer

Fig. 2.8 Raman Spectrometer

Raman spectroscopy of the studied ceramics are carried out using Raman spectrometer (HEDA URSM4/5/7, Korea) with laser excitation wavelength 473 nm. The Raman spectrometer is specified with Excitation Laser Sources (457nm/ 532nm/ 785nm), Olympus microscope (Magnification – 5X, 20X, and 100X), detector (CCD) and the gratings with spectral ranges from 0 to 3600 cm^{-1}.

2.4.4 P-E loop Measurement

Fig. 2.9 P-E Loop set up

Polarization -Electric Field (P-E) hysteresis loops measurements were recorded using precision premier II P-E loop tracer, from Radiant Technologies. The The Precision Premier II is offered in a ±10V, 30V, 100V, 200V, and 500V built-in drive volt option. The Precision Premier II can be expanded to 10kV with the addition of a high voltage interface and amplifier. The Premier II tester makes testing of thin films and bulk ceramics a fast and simple process. However, P-E loop measurement follows Sawyer-Tower circuit principle.

CHAPTER 3

RESULTS AND DISCUSSION

3.1 Introduction:

Barium strontium zirconium titanate (BSZT) powders were synthesized using solid state reaction method. And the phase analysis of the prepared powders was performed using X-ray diffractometer. The powders with pure phase were compressed into pallets of a diameter 10mm using hydraulic press at a pressure of 100MPa. These pallets were then sintered at temperature 1250°C for 2 hours. In this chapter a systematic study of structural, dielectric and ferroelectric properties of synthesized BSZT ceramics is presented.

3.2 X-ray diffraction (XRD) analysis:

Fig. 3.1a) displays the X-ray diffraction pattern of the prepared $Ba_{0.7}Sr_{0.3}Zr_{x}Ti_{1-x}O_3$ samples with different Zr (x=0.04, 0.08, 0.12). The diffraction patterns of all the prepared ceramics demonstrate the formation of the expected perovskite phase. No extra peaks suggest the non-existence of any secondary phases. To get more information from the XRD data, the diffraction peak at 39◦ was magnified for the ceramics with different Zr compositions, as shown in Fig. 3.1a). The sharp and clear peaks of the prepared BSZT powders indicate the crystalline nature of the sample. The standard JCPDS database No.01-089-0274 was used to index the diffraction peaks for the compositions under study.

In order to determine the lattice parameters, Rietveld refinement of the prepared sample was carried out using the xrd data (fig. 3.1b-d). According to the Rietveld refinement, the lattice parameters increase with increasing Zr doping in barium strontium zirconium titanate (BSZT) samples because ionic radius of Zr^{4+} (0.72 Å) is larger than ionic radius of Ti^{4+} (0.605 Å). Zr replaces Ti in the BSZT structure to provide a larger unit cell, increasing the interplanar distance and in turn, the lattice parameter [36].

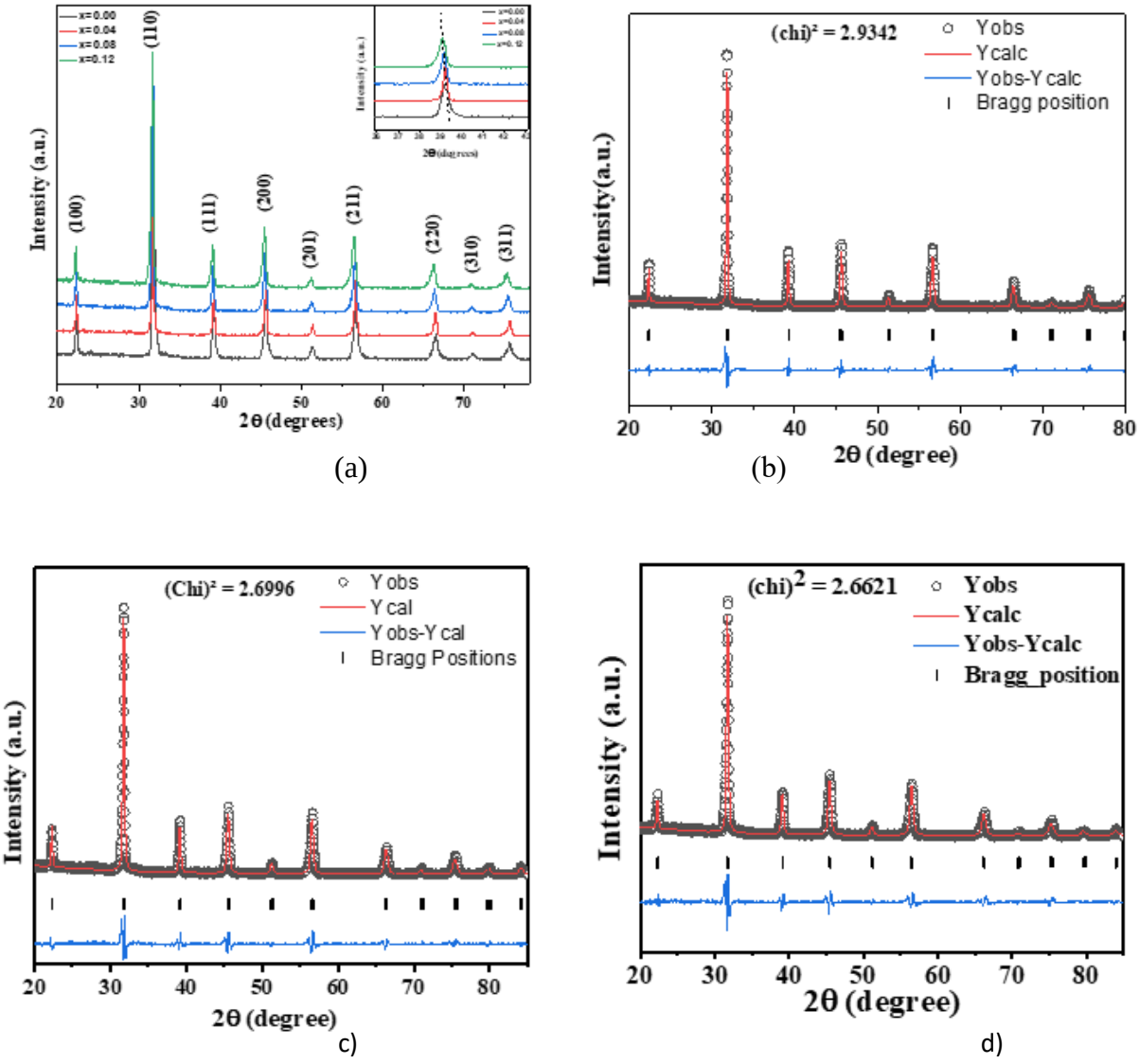

Fig 3.1 (a). XRD pattern, (b-d). Rietveld refinement of $Ba_{0.7}Sr_{0.3}Zr_xTi_{1-x}O_3$ ceramics with varying Zr as (x=0.00, 0.04, 0.08, 0.12)

Table 3.1 lattice parameters and volume of $Ba_{0.7}Sr_{0.3}Zr_xTi_{1-x}O_3$ (x=0.04, 0.08, 0.12)

Composition	Chi^2	*Lattice Parameters*	*Volume*
BSZT4	2.93	a=3.9734 b=3.9734 c=3.9879	62.961
BSZT8	2.70	a=3.9893 b=3.9893 c=3.9771	63.293
BSZT12	2.66	a=3.9976 b=3.9976 c=3.9843	63.672

3.3 Raman spectroscopy

Fig. 3.2 illustrates the room temperature Raman spectra of $Ba_{0.7}Sr_{0.3}Zr_xTi_{1-x}O_3$ ceramics with (x=0.04, 0.08, 0.12). Due to lattice distortion from the incorporation of Zr and Sr ions, positions and intensities of the characteristic Raman peaks are slightly different. The dip at 166.32cm^{-1} in the Raman spectrum for x= 0 is more visible than that for x= 0.04, x= 0.08 and for x= 0.12 it is barely present.

The frequency modes below 200 cm^{-1} may be associated with the vibration modes of the A-site cations. The vibrational modes at approximately 150 cm^{-1} and 175 cm^{-1} are attributed to the Ba–O/Sr–O bond vibrations [37]. There are strong correlations between the Ti–O bond vibrations and the dielectric behavior. The frequency mode region around 200–400 cm^{-1} is generally believed to influence the dielectric properties in perovskite-structured systems

The modes in the high-frequency region, which is above 700 cm^{-1} are associated with the merged bands of A_1 (longitudinal optical) and E (longitudinal optical). Furthermore, it can

be observed from Fig. [3.5] that these modes shift toward the lower wavenumber range (700–900 cm^{-1}), as the zirconium content increases.[38]

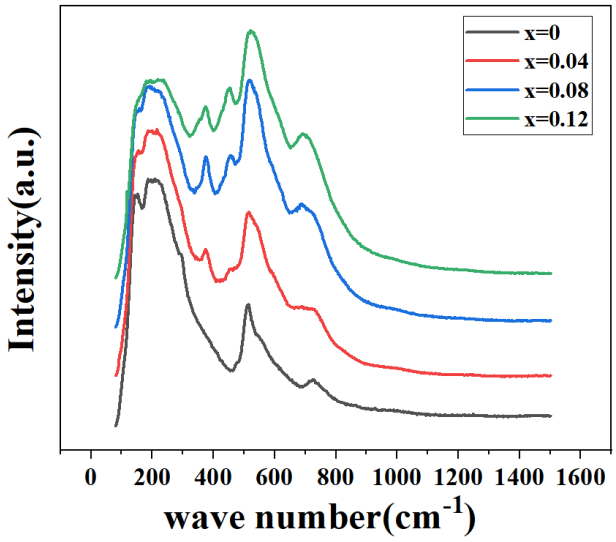

Fig 3.2 Raman spectra for $Ba_{0.7}Sr_{0.3}Zr_xTi_{1-x}O_3$ (x=0.04, 0.08, 0.12) at room temperature.

3.4 Dielectric Properties

Dielectric measurements were performed on BSZT ceramics at room temperature that were sintered at 1250°C for 2 hours. Figures 3.3a and 3.3b display the dielectric constant and dielectric loss over a frequency range of 100 Hz to 1 MHz, respectively. At lower frequencies, all samples exhibited a high dielectric constant which is a common

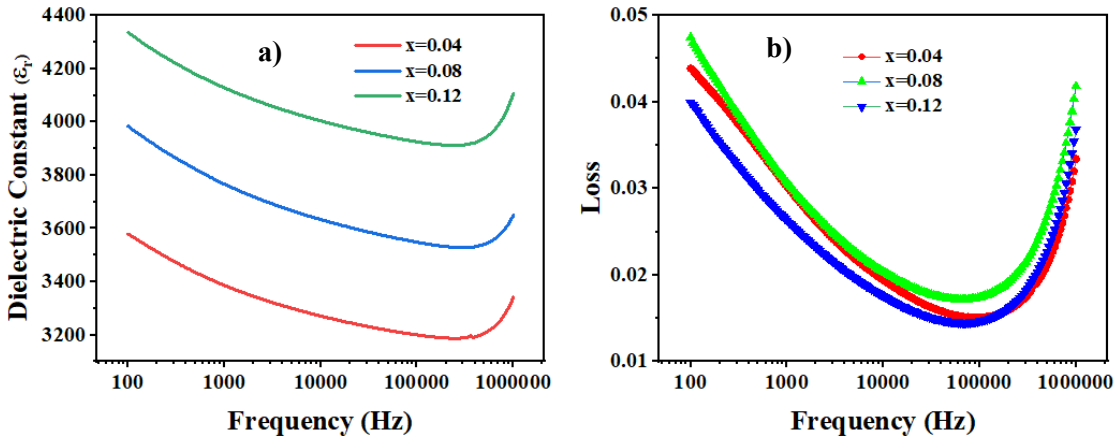

Fig 3.3 (a and b). Variation of dielectric constant and dielectric loss with frequency respectively.

characteristic across different compositions. This behaviour is due to the presence of various polarization mechanisms such as electronic, orientational, interfacial, and ionic—that contribute to the overall polarization. As the frequency increases, these mechanisms become less effective, leading to a decrease in the dielectric constant.

From fig. 3.2 b) it is observed that the dielectric loss decreases with increasing frequency upto a certain point (around 100 KHz), which starts increasing again afterwards. Higher dielectric loss is observed at low frequencies may be due to space charge polarization. At high frequencies, dipoles cannot follow the rapid change in the electric field, therefore there is increased loss. Substituting Zr into the BSZT ceramics improved the frequency stability of the dielectric constant and significantly reduced the dielectric loss. These enhanced dielectric properties make the BSZT composition promising for applications in capacitors and energy storage devices.[39]

3.5 Ferroelectric properties

Fig 3.4 shows the P-E loop of the $Ba_{0.7}Sr_{0.3}Zr_xTi_{1-x}O_3$ ceramics with (x=0.04, 0.08, 0.12) at room temperature. The P-E loop measurement of BSZT ceramics were done at 10 Hz. Formation of hysteresis loop shows ferroelectric nature of the prepared BSZT samples.

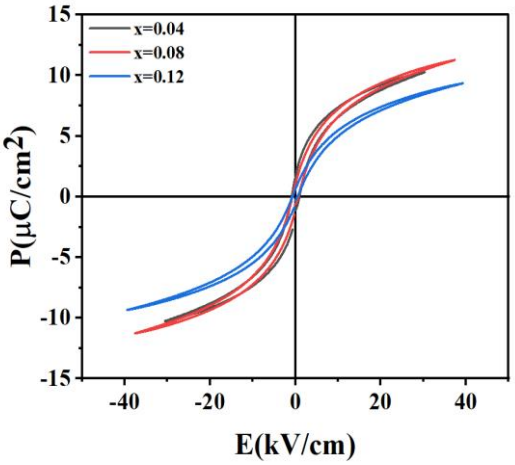

Fig. 3.4 PE hysteresis loop of prepared $Ba_{0.7}Sr_{0.3}Zr_xTi_{1-x}O_3$ samples with varying Zr as (x=0.04, 0.08, 0.12)

From the PE loop data, all the energy storage parameters are calculated for the as prepared $Ba_{0.7}Sr_{0.3}Zr_xTi_{1-x}O_3$ ceramics with (x=0.04, 0.08, 0.12) as shown in the fig. 3.5(a-c). This demonstrates the recoverable energy density changes with changes in zirconium content.

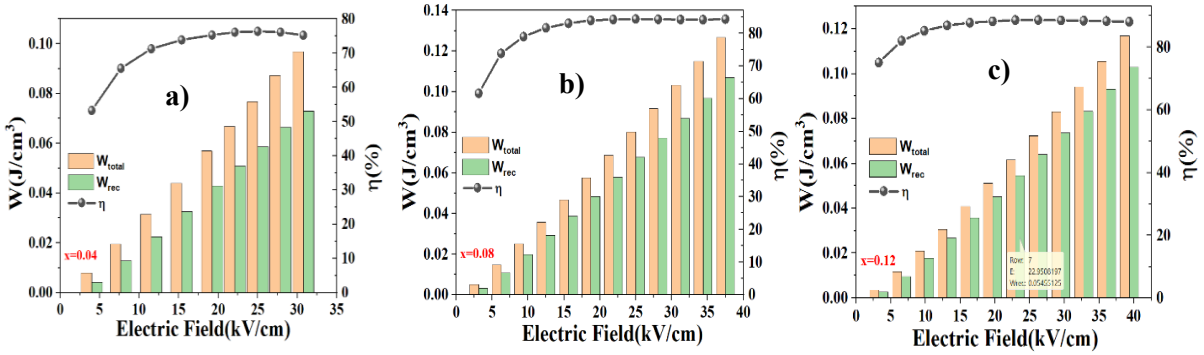

Fig 3.5(a-c) Energy storage density plot for prepared $Ba_{0.7}Sr_{0.3}Zr_xTi_{1-x}O_3$ ceramics (x=0.04, 0.08, 0.12)

The sample with composition x= 0.04 has the lowest recoverable energy density (W_{rec}= 0.028 J/cm^3) and the minimum energy efficiency (75%) among all the studied ceramics. For x= 0.08, W_{rec} is 0.102 J/cm^3 and energy efficiency is 84%. However, a maximum W_{rec} and energy efficiency of 0.106 J/cm^3 and 88% is achieved respectively for x=0.12. Therefore, one can finalize that as the Zr doping increases, the recoverable energy density and energy efficiency increases.

CHAPTER 4

CONCLUSIONS AND FUTURE SCOPE

4.1 Conclusions

The goal of this study was to investigate the energy storage capacity of Sr and Zr co-doped Barium Titanate (BSZT) ceramics through their synthesis and characterization. To improve thermal stability and dielectric performance, the perovskite structure of Barium Titanate ($BaTiO_3$) was altered by replacing Zr at the Ti site and Sr at the Ba site. Pure phase BSZT samples could be prepared in a dependable and economical manner using the solid-state synthesis approach. The creation of a single-phase perovskite structure with minor alterations in peak positions was confirmed by structural investigation using X-ray diffraction (XRD), confirming effective doping. Raman spectroscopy verified the impact of Sr and Zr on lattice. Also the improved energy storage efficiency is observed with Zr doping. Overall, the findings show that doping barium titanate with Sr and Zr is a useful technique for customizing the material's characteristics for energy storage devices. The optimized BSZT ceramics are interesting options for multilayer ceramic capacitors (MLCCs) and next-generation electronic components because they show a good balance between ferroelectric characteristics and dielectric efficiency.

4.2 Future Scope

Following recommendations are made for the extension of the present work:

1) Composition Optimization: - Additional adjustment of the Ba/Sr and Zr/Ti ratios can improve the dielectric and ferroelectric qualities and assist customize the phase stability, enabling the material for more specialized uses.

2) Thin Film Development: - In order to investigate thickness-dependent properties and incorporate them into microelectronic devices, thin films can be created using methods such as sol-gel or PLD.

3) Using Transition or Rare Earth Elements for Doping: Further doping (e.g., with La, Mn, or Nb) could enhance thermal stability, breakdown strength, and energy storage density

4) Applications of Energy Storage: - When properly optimized, BSZT may find application in sophisticated energy storage systems such as electrocaloric cooling devices and pulsed power capacitors.

REFERENCES

[1] D. Damjanovic, “Ferroelectric, dielectric and piezoelectric properties of ferroelectric thin films and ceramics,” Reports on Progress in Physics, vol. 61, no. 9, pp. 1267–1324, Sep. 1998, doi: 10.1088/0034-4885/61/9/002.

[2] M. E. Lines and A. M. Glass, Principles and applications of Ferroelectrics and related materials. 2001. doi: 10.1093/acprof:oso/9780198507789.001.0001.]

[3] Y. Saito et al., “Lead-free piezoceramics,” Nature, vol. 432, no. 7013, pp. 84–87, Oct. 2004, doi: 10.1038/nature03028.

[4] Libretexts, “Dielectric polarization,” Engineering LibreTexts, Oct. 27, 2021. https://eng.libretexts.org/Bookshelves/Materials_Science/Supplemental_Modules_(Materials_Science)/Optical_Properties/Dielectric_Polarization

[5] “Piezoelectricity - an overview | ScienceDirect Topics,” www.sciencedirect.com. https://www.sciencedirect.com/topics/chemistry/piezoelectricity

[6]Wikipedia contributors, “Pyroelectricity,” Wikipedia, Apr. 20, 2025. https://en.wikipedia.org/wiki/Pyroelectricity

[7] “Ferroelectric Material - an overview | ScienceDirect Topics,” www.sciencedirect.com. https://www.sciencedirect.com/topics/materials-science/ferroelectric-material

[8] “Physics 122 | Welcome to Physics 122.” https://122.physics.ucdavis.edu/

[9] “Understanding a ferroelectric hysteresis loop in electronics,” Oct. 15, 2020. https://resources.pcb.cadence.com/blog/2020-understanding-a-ferroelectric-hysteresis-loop-in-electronics

[10] G. K. Sahoo, “Synthesis and Characterization of BaTiO3 Prepared by Molten Salt Synthesis Method,” Jan. 01, 2009. https://www.researchgate.net/publication/37394599_Synthesis_and_Characterization_of_BaTiO3_Prepared_by_Molten_Salt_Synthesis_Method

[11] J. Zhao, “First-principles study of ferroelectricity in oxide superlattices,” Oct. 11, 2013. https://www.researchgate.net/publication/281184657_First-principles_study_of_ferroelectricity_in_oxide_superlattices

[12] A. Rotaru and F. D. Morrison, “Vogel–Fulcher analysis of relaxor dielectrics with the tetragonal tungsten bronze structure: Ba6MNb9O30 (M = Ga, Sc, In),” Journal of Thermal Analysis and Calorimetry, vol. 120, no. 2, pp. 1249–1259, Jan. 2015, doi: 10.1007/s10973-014-4355-5.

[13] T. Connor et al., “Pyrochlore compounds from atomistic simulations,” Frontiers in Chemistry, vol. 9, Nov. 2021, doi: 10.3389/fchem.2021.733321

[14] Z. Liu, H. Wu, W. Ren, and Z.-G. Ye, “Piezoelectric and ferroelectric materials: Fundamentals, recent progress, and applications,” Comprehensive Inorganic Chemistry III, pp. 135–171, 2023, doi: https://doi.org/10.1016/b978-0-12-823144-9.00069-8.

[15] S. Shalu and B. Dasgupta Ghosh, “Synthesis, characterisation and dielectric properties of low-loss Zr-doped barium strontium titanate materials,” Advances in Applied Ceramics, vol. 118, no. 8, pp. 451–457, Sep. 2019, doi: https://doi.org/10.1080/17436753.2019.1664793.

[16] S. Esmaeili, M. H. Ehsani, D. Toghraie, and S. Saber-Samandari, “Sr-doping effects on piezoelectric and dielectric properties of lead-free barium titanate via molecular dynamics approach,” Scientific Reports, vol. 15, no. 1, Mar. 2025, doi: 10.1038/s41598-025-92959-w.

[17] Y. Saito et al., “Lead-free piezoceramics,” Nature, vol. 432, no. 7013, pp. 84–87, Oct. 2004, doi: 10.1038/nature03028.

[18] F. Kawamura, M. Kamei, I. Yasui, and I. Sunagawa, “Effect of impurity cations on the growth and habits of SNO2 crystals in the SNO2-CU2O flux system,” Journal of the American Ceramic Society, vol. 82, no. 3, pp. 774–776, Mar. 1999, doi: 10.1111/j.1151-2916.1999.tb01834.x.

[20] S. Mueller et al., “Incipient ferroelectricity in Al-Doped HFO2 thin films,” Advanced Functional Materials, vol. 22, no. 11, pp. 2412–2417, Mar. 2012, doi: 10.1002/adfm.201103119.

[21] J. A. Kers et al., “Nitration of a peptide phytotoxin by bacterial nitric oxide synthase,” Nature, vol. 429, no. 6987, pp. 79–82, May 2004, doi: 10.1038/nature02504.

[22] C. G. Treviño-Palacios et al., “Intensity dependent mode competition in second harmonic generation in multimode waveguides,” Applied Physics Letters, vol. 67, no. 2, pp. 170–172, Jul. 1995, doi: 10.1063/1.114656.

[23] L. Liu, J. Zhang, and Y. Wang, “Addressing a novel paradigm toward high energy storage,” The Innovation Materials, vol. 2, no. 4, p. 100103, Jan. 2024, doi: 10.59717/j.xinn-mater.2024.100103.

[24]K. Xu, L. Yang, J. Wang, and H. Huang, “Design of high energy storage ferroelectric materials by phase-field simulations,” Journal of Materials Informatics, vol. 5, no. 2, Mar. 2025, doi: 10.20517/jmi.2024.97.

[25] Q. Chai et al., “Excellent energy storage properties in lead-free ferroelectric ceramics via heterogeneous structure design,” Nature Communications, vol. 16, no. 1, Feb. 2025, doi: 10.1038/s41467-025-56767-0.

[26] H. Kishi, Y. Mizuno, and H. Chazono, “Base-Metal Electrode-Multilayer Ceramic Capacitors: Past, Present and Future Perspectives,” Japanese Journal of Applied Physics, vol. 42, no. Part 1, No. 1, pp. 1–15, Jan. 2003, doi: 10.1143/jjap.42.1.

[27] “Solid state chemistry,” Elsevier Shop. https://shop.elsevier.com/books/solid-state-chemistry/ropp/978-0-444-51436-3

[28] “Solid State Chemistry and its Applications, 2nd Edition,” Wiley.com. https://www.wiley.com/en-us/Solid+State+Chemistry+and+its+Applications%2C+2nd+Edition-p-9781118695579

[29] “Welcome To Zscaler Directory Authentication,” Researchgate.net, 2025. https://www.researchgate.net/figure/Schematic-illustration-of-Braggs-Law_fig1_48172215

[30] Dinnebier, R. E., & Billinge, S. J. L. (2008). Powder Diffraction: Theory and Practice.Final plot of the Rietveld refinement, showing the observed, calculated.

[31] Ferraro, J. R., Nakamoto, K., & Brown, C. W. (2003). Introductory Raman Spectroscopy (2nd ed.). Academic Press.Raman Spectroscopy: Principle, Instrumentation and Applications

[32] “MIT OpenCourseWare,” MIT OpenCourseWare. https://ocw.mit.edu/

[33] Reda, M., El-Dek, S.I. & Arman, M.M. Improvement of ferroelectric properties via Zr doping in barium titanate nanoparticles. *J Mater Sci: Mater Electron* **33**, 16753–16776 (2022). https://doi.org/10.1007/s10854-022-08541-x

[34] Integrated structural and functional analysis of Ba1-xSrxTiO3-Bi0. 5Na0. 5TiO3 ceramics: Insights into energy storage and electrocaloric performance AR Sahoo, VR Reddy, O Subohi - Ceramics International, 2024

[35] Integrated structural and functional analysis of Ba1-xSrxTiO3-Bi0. 5Na0. 5TiO3 ceramics: Insights into energy storage and electrocaloric performance AR Sahoo, VR Reddy, O Subohi - Ceramics International, 2024

[36] S. Shalu and B. Dasgupta Ghosh, “Synthesis, characterisation and dielectric properties of low-loss Zr-doped barium strontium titanate materials,” Adv. Appl. Ceram., vol. 118, no. 8, pp. 451–457, Sep. 2019.

[37] J. P. Singh and R. S. Katiyar, “Raman scattering study of Zr-doped $Ba_{0.8}Sr_{0.2}TiO_3$ ceramics,” J. Appl. Phys., vol. 115, no. 5, Art. no. 054102, Feb. 2014.

[39] S. Li, Y. Wang, M. Yang, J. Miao, K. Lin, Q. Li, X. Chen, and X. Xing, “Ferroelectric thin films: performance modulation and application,” Mater. Adv., vol. 3, pp. 1234–1250, May 2022.